Turkish Computational and Theoretical Chemistry

Turkish Comp Theo Chem (TC&TC)

Volume(Issue): 9(2) – Year: 2025 – Pages: 77-95

e-ISSN: 2602-3237

https://doi.org/10.33435/tcandtc.1501142

Received: 14.06.2024 ***Accepted***: 19.09.2024 *Research Article*

Theoretical Study of Structure and Acidity of Uric Acid and its Metal Complexes: M(UA)+n (M= Li^{+}, Be^{++}, Na^{+}, Mg^{++}, K^{+}, Ca^{++}) and M(UA)2+n (M= Zn^{+2}, Cd^{+2}, Cu^{+}, Ag^{+})

Meriem HAFIED[a,b,1],Mohammed AICHI[b,c]

[a]Department of medicine, Faculty of medicine, University of Batna2, Algeria.
[b]Laboratory of chemistry of materials and living organisms: Activity-reactivity (LCMVAR).
[c]Department of Mater Sciences, Faculty of Sciences and Technology, University of Khenchela, Algeria.

Abstract: Uric acid (UA) is a biological molecule which is susceptible to be investigated theoretically. A theoretical investigation is carried out in the gas phase and by water effect at the ground state by using density functional theory method (DFT) at the B3LYP/6-31(d) and B3LYP/ LANL2DZ levels on the structure of different chemical forms of Uric Acid (UA) and its metal complexes. Solvent effect (water) is included using the polarizable continuum model (PCM). Neutral structures (ketonic, enolic, dimeric, monohydrate) and anionic structures has been fully optimized. Furthermore, and in order to estimate the Brönsted acidity of (UA), the interaction of both enolic and ketonic forms with alkali meta cations (Li^{+}, Na^{+}, K^{+}, Be^{++}, Mg^{++}, Ca^{++}) was calculated in $M(UA)^{+n}$ complex structures. Proton acidity of (UA) and its complexes was estimated by calculating deprotonation energy (DE) and δ (ppm)$^{1}{}_{1}$H NMR chemical shift using GIAO method. Metal cations effects on distinct N-H and O-H stretching vibrational modes of studied structures have also been examined. Further, we explored the geometry, and acidity of several uric acid transition metal complexes $M(UA)_{2}^{+n}$ (M= Zn^{+2}, Cd^{+2}, Ag^{+}, Cu^{+}) in water. The complex was calculated using mixed basis set 6-31G(d) and LANL2DZ (on the transition metal).

Keywords: Uric acid (UA), chemical forms, water, acidity, metal complex $M(UA)_{2}^{+n}$.

1. Introduction

Uric acid (UA) is a heterocyclic organic compound (imidazole (I) and pyrimidine (II) rings) **(Figure.1)** its name is (7,9-Dihydro-1H-purine-2,6,8(3H)-trione) [1]. It was first discovered by Swedish Chemist Carl Wilhelm Scheele in the year 1776 [2] when he successfully isolated uric acid from kidney stones. Though it was discovered in the year 1776 it was synthesized for the first time in the year 1882 by Ukrainian chemist Ivan Horbaczewski. He synthesized uric acid by melting urea and glycine [3].

Uric acid is the end product of purine breakdown in humans. It is removed by renal action of which 90% is reabsorbed with the remained excreted in urine [4]. It has been used as a diagnostic marker of many diseases; for example, a high level of serum uric acid is often associated with gout, diabetes, and metabolic syndrome [5]. Uric Acid (UA) is one of the most intriguing chemicals in the human body that may be studied theoretically and many theoretical and experimental studies was carried on its structure [6,7,8]. Several studies have concluded that uric acid (UA) is a naturally occurring antioxidant [9]. It is the ultimate oxidation product of purine metabolism and is generally eliminated in urine. Gout is caused by an excess of uric acid in the tissues [10]. This condition is characterized by the deposition of massive crystalline aggregates in joints, resulting in excruciating discomfort.

Both *in vitro* and *in vivo* studies have demonstrated that (UA) is an effective scavenger of hydroxyl and peroxynitrite radicals Uric acid ionizes with pKa at pH 5.75 In the extracellular fluid, at physiological pH of 7.4, uric acid is mainly in the ionized form of urate, while in the urine, which is

[1] Corresponding Authors
e-mail: hafied_meriem@yahoo.fr

usually acidic, the un-ionized uric acid form predominates

Additionally, and due to the ability of the Uric acid (UA) molecule to form rather stable metal complexes, as well as more of previous investigations [14], [15], [16], [17] on (UA) metal complexes studies.

UA's keto-enol tautomerism **(Figure 2.)** has been the topic of various studies. In addition, the solid state of (UA) is distinguished by a planar tri-keto structure [18]. The acidity of (UA) seems to be a very interesting property, although this molecule has been the subject of several theoretical and experimental research [19]. In this regard, and despite the fact that (UA) has four acid protons, the experiment, however, showed only two possible acidity and thus, Uric acid (UA) is a weak diprotic acid with an aqueous pKa1 of 5,4 and pKa2 of 9,8. To explore all four acidities, or to clarify the existence of these two acidities, the present work is interested to investigate theoretically the structure and the charge density of Uric acid (UA) and its chemical forms for clarifying Brønsted acidity [20].

Furthermore, we are very interested, on the structure of alkali metal complexes $M(UA)^{+n}$ to examine O-H and N-H Bronsted acidity by combining DFT with the PCM continuum solvent model [21,22].

Deprotonating Energy and δ NMR $^{1}_{1}H$ chemical shift, as well as other parameters like charge of protons and the stability of the corresponding anions, are frequently employed to estimate the proton acidity. Alkali metal cations Li^{+}, Na^{+}, K^{+}, Be^{++}, Mg^{++}, Ca^{++} are used in our investigation to predict the varying stability and acidity of the various (UA) complexation by calculating HOMO and LUMO energies and their gaps $\Delta E_{HOMO\text{-}LUMO}$. Moreover, Natural Bond Orbital (NBO) [23] analysis was performed on the optimized structures to obtain a further insight into the electronic properties of the system.

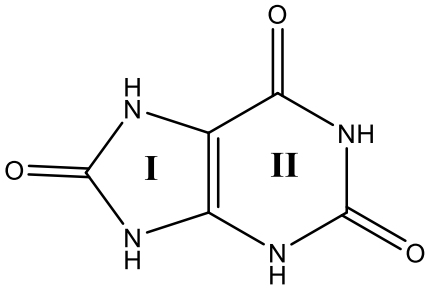

Figure 1. Uric acid structure

Beyond and above this complexity, Olga et al. [24] have been studied experimentally a series of metal uric acid complexes. These complexes were synthesized using different metal ions of Zn^{+2}, Cd^{+2}, Hg^{+2} and Ag^{+} in aqueous solution. Obtained UA-metal $[M(UA)_2]^{+2}$ complexes structures and locating complexation sites were explored on the basis of Density Functional Theory calculations using B3LYP/6-31G(d,p) and LANL2DZ for Ag, Zn, Cu, and Cd atoms.

Furthermore, due to the weak energy between the ketonic and the enolic form in the keto-enol equilibrium, the contribution, that we make in this study and the task which has never been done by any other study before, is to include the two forms of uric acid in the investigation of their acidities, and consequently we have performed all calculations by introducing (UA) structure in its two forms.

2. Computational Method

The geometry optimization and single point energy calculations at the ground stats were computed using Gaussian16 software program [25] through the hybrid density functional B3LYP/6-31G(d) and B3LYP/LANL2DZ basis sets to predict the molecular structure and vibrational wavenumbers. We have employed B3LYP [26,27] functional with mixed basis set 6–31G(d) and LANL2DZ (on the transition metal) to further predicting two important molecular properties: deprotonation energy (ED) and heat of deprotonation (HD). In addition, we have used the polarisable continuum model (PCM) for implicit water solvation [28] in the Gaussian16 program for the geometry of (UA) chemical forms and its metal complexes in aqueous solution. NMR $^{1}_{1}H$ Chemical shift δ(ppm) were calculated by using GIAO (Gauge Including Atomic Orbitals) method [29]. in Gauss View06 by choosing TMS HF/6-

31G(d) GIAO reference. Delocalisation of charge density has been estimated by NBO (Natural Bond Orbithal) method. Deprotonation energy [30,31], which can be defined as the enthalpy change associated with the gas phase deprotonation reaction, $AH \rightarrow A^- + H^+$, has been calculated in this work only for the most acid proton.

3. Results and discussion

3.1. Chemical forms of Uric Acid (UA)

Uric Acid (UA) can exist in its molecular form at the ketonic and enolic structures in tautomeric equilibrium [32] **Figure 2.**, and thus in monoanionic, di-anionic forms, dimeric form and monohydrated forms [33].

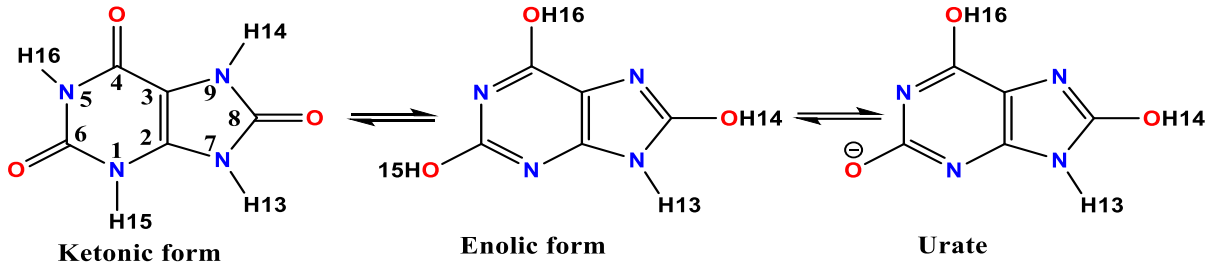

Figure 2. keto-enolic equilibrium of (UA) and Urate

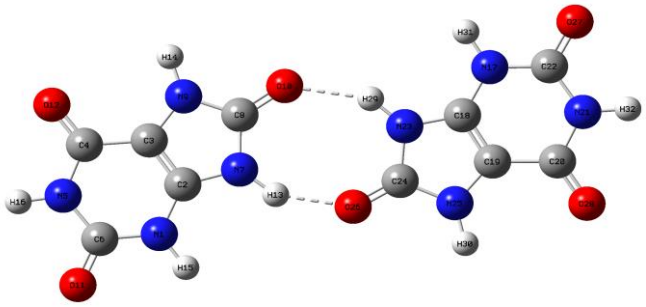

Figure 3. dimer of uric acid with a pseudo eight-membered ring.

Table 1. The main parameters of ketonic and enolic forms of Uric Acid (UA)

Structures	E_T (Hartree)	E_{HOMO} (eV)	E_{LUMO} (eV)	$\Delta E_{HOMO-LUMO}$ (eV)	μ_{Total} (Deby)
(UA)-Keto (g)	-637,671875	-5.909	-0.912	4.997	3,0468 Exp [2,8]
(UA)-Keto(water)	-637,695461	-5.733	-0.740	4.992	4,2444 Exp [5,5]
(UA)-Enol (g)	-637,622385	-5.860	-0.412	5.447	5,2054
(UA)-Enol(water)	-637,646261	-5.995	-0.561	5.434	6,7651

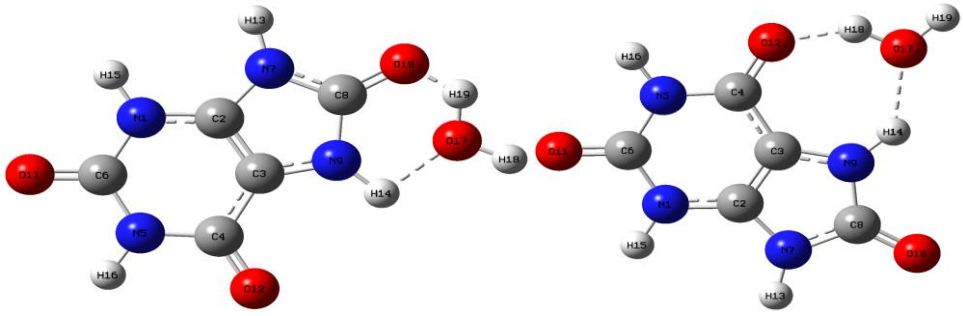

(a) **(b)**

Figure 4. monohydrated of uric acid **(a)** pseudo six-membered ring, **(b)** with a pseudo seven-membered ring.

Depending on the pH of the medium in which the uric acid is found, the equilibrium will be shifted towards the formation of the molecular form for a pH < pKa or towards the ionized form for a pH > pKa [22].

At physiological pH (7,35-7,45), uric acid is 98% in ionized form. It is present at 37°C in plasma in the form of sodium urate. Uric acid and urate are relatively insoluble molecules that easily precipitate in aqueous solutions such as urine or synovial fluid, which can cause lithiasis or arthritis. The uric acid/urate ratio increases when the acidity of the environment decreases.

3.2. Mono-hydrated and dimeric forms of (UA)

Uric acid exists primarily in two crystalline forms, anhydrous and dihydrate. The first predominates in lithiasis, the second in stones. It is considered that the dihydrate form is, in the majority of cases, the initial phase and that it then converts quite quickly to the anhydrous form [34].

In the dimeric system (**Figure 3.**), two uric acid (UA) molecules are joined by two hydrogen bonds. All the while, a pseudo-cycle with eight-member ring is formed, adding to the stability of this chemical structure. This geometry gives the possibility that the two molecules are once donors and once acceptors of protons.

Uric Acid (UA) and a water molecule may interact to produce two similar monohydrate systems in which two hydrogen bonds appear forming either a six-membered ring pseudo-cycles **(a)** or Seven-membered ring pseudo-cycles **(b)**. (**Figure .4**)

The enolic form have been excluded from much work that involves the structure of Uric Acid in their studies because it is more reactive. Although the enolic form is less stable but the keto-enolic tautomeric equilibrium does not cost much energy. For this purpose, we preferred to set up both structures simultaneously.

The novelty and the contribution that this study brings is the incorporation of the enolic form of Uric Acid in the different calculations carried out, and this for the reasons that can be given in the following paragraph.

The geometry optimization of the ketonic and enolic forms indicates an energy difference equal to (0,05 Hartree) 1,346 Kcal/mol and (0,0492 Hartree) 1,339 Kcal/mol in the gas phase and in the aqueous phase respectively estimated at B3lyp/6-31g(d) level. The ketonic form is the most stable on the potential energy surface. The enolic form, on the other hand, is less stable; it represents a local minimum and thus it is a stable intermediate. The energy between the ketonic and enolic form was estimated at the same level of calculation at 1,767 kcal/mol which is comparatively a very weak barrier energy. Therefore, we can conclude that these two forms can exist at the same time in a tautomeric equilibrium.

In addition, The IR vibrations provides some findings on the stability and reactivity of uric acid UA. In the following discussion, UA in its enol form provides as a result the minimal frequencies correspond to the mixed deformation out of plan (the O10-H14 bond has a relatively large magnitude, whereas the N7-H13 bond has a modest amplitude).

However, the minimal frequencies correspond to the deformation out of plane of tow rings in the ketonic form of (UA) either in gas phase or in water. Electrostatic surface potential ESP map of UA can be used to distinguish between electron-rich zone (in red color) that receives electrophilic attack and electron-poor (in blue color) which undergoes electrophilic attack region. **Figure 5.**

The largest interval of electron density has been found for UA-Keto structure, and it tends to be between ∓ 9.249e-2. While the restraint interval of electron density characterizes UA-enol form and it tends toward ∓0.127e0.

It is interesting that the dipole moment of neutral Uric Acid was increased from the gas phase (μ=2.8 D) to a water environment (μ=5.5 D) [35], While, the charge transfer, reflected by $\Delta E_{HOMO\text{-}LUMO}$ gap in gas phase and in water, are similar.

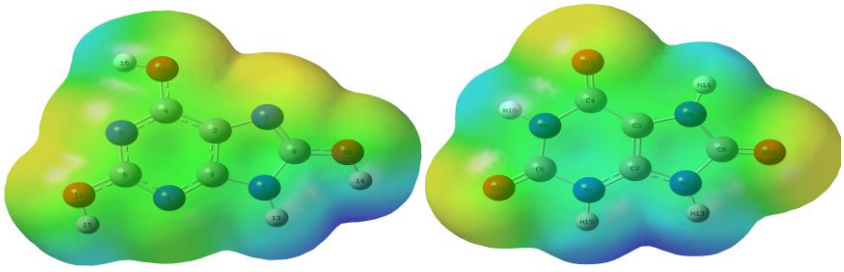

ESP UA-enolic **ESP UA-ketonic**

Figure 5. electrostatic surface potential map ESP of UA forms

Table 2. δNMR 11H chemical shift (ppm) and deprotonation energy DE (Kcal/mol)

Structures	δH13	δH14	δH15	δH16	DE
(UA)-Keto (g)	5,50	5,67	5,71	**6,23**	365.04
(UA)-Keto(water)	6,41	6,01	**6,63**	6,47	304.39
(UA)-Enol (g)	**6,49**	4,07	5,36	5,65	348.90
(UA)-Enol(water)	**7,51**	5,48	5,94	6,03	304.85

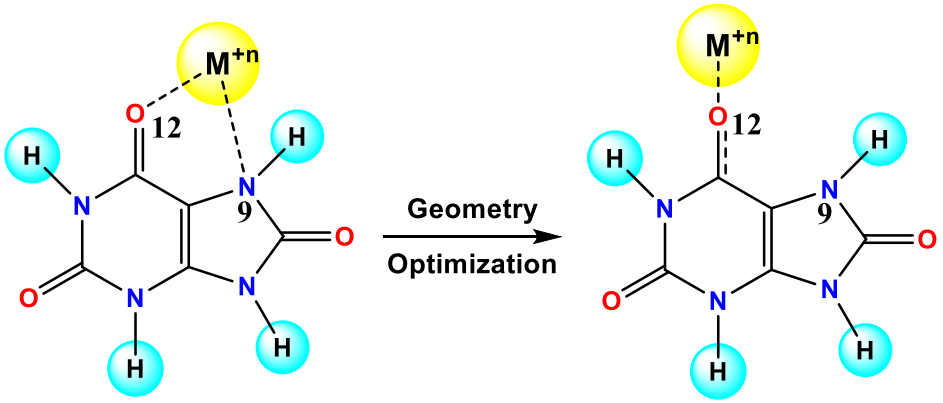

Figure 6. Complexation of (UA)-Keto with Na^+, Li^+, K^+, Be^{++}, Mg^{++}, and Ca^{++} metal cations

Therefore, according to the tautomeric keto-enolic equilibrium, the tow acidity observed in uric acid (UA) that were investigated in vitro [36] depends on the loss of two protons coming from two forms of (UA). According to our results in water **Table 2.,** the first acidity is obtained by the deprotonation of H15 in the ketonic form, whereas the second is by the deprotonation of H13 in the enolic form.

3.3. IR vibrations of C=O, N-H and O-H bonds

The fundamental IR bands, in gas phase and in water, of (UA) in its ketonic and enolic forms are listed in **Table 3.** and **Table 6.** Ketonic form has major peaks in the range starting with 1783,40 cm^{-1} of C4=O12 and ending with 3678,81 cm^{-1} stretching bonds. 1858,81 cm^{-1} for C=O of the imidazole ring, and tow frequencies C=O 1816,95 cm^{-1} , 1783,40 cm^{-1} for pyrimidine ring.

In the case of enolic form the three frequencies of O-H and one frequency of N-H stretching bonds are 3781,28 cm^{-1}, 3730,12 cm^{-1}, 3687,31 cm^{-1}, 3654,62 cm^{-1}.

3.4. Acidity in alkali metal complexes of Uric $[M(UA)]^{+n}$ M=Li^+, Mg^{++}, K^+, Ca^{++}, Na^+, Be^{++}

Uric acid is a weak diprotic acid (has two dissociable protons) with pKa1≈5.4 and pKa2≈10.3. At the physiologic pH of 7.4, [37]. Nevertheless, because there are four protons in Uric Acid (UA) structure, these four acidities might be discussed and we may estimate them by calculating of the δNMR $^1{}_1H$ chemical shift and the deprotonation energy (DE) parameters. Additionally, we explored the impact of mono and divalent alkali metal complexation on the Bronsted acidity force of the four protons. We have chosen Li^+, Na^+, K^+, Be^{++} $Mg^{++,}$ Ca^{++} alkali metal cations to interact as Lewis acid with the (UA) structures, and therefore we generate some adducts in which the complexation sites in UA act as an electron pair donor through oxygen or nitrogen atoms.

At first, and based on molecular modelling calculations, complexation of alkali metals has been shared between N9 and O12 sites of the ketonic form **Figure 6.** Geometry optimization calculation at the B3LYP/6-31G(d) level of all complexes provides the structures shown in **Figure 7.** We followed and compared the shielding chemical shift of the protons by the GIAO method. Results are obtained at TMS B3LYP/6-311+G (d) GIAO in Gaussian16 [25].

Geometry of isolated uric acid (UA) without any other interaction is employed as a starting point to compare it with the other metal complexes. We can estimate the charges labelled the four hydrogens, the chemical shift as well as the interval of the electrostatic potential by the case of the interaction of UA with the different alkali metal cations Li^+, K^+, Na^+, Be^{++}, Mg^{++}, Ca^{++} that form several adducts **Figure 7.**

Geometry optimization generates the structures of these adducts and consequently the choice of the alkali metals to coordinate with the oxygen atom O12 rather than the nitrogen atom N9 makes the alkali metals as monocoordinated by selecting one interaction site **Figure 6.** (UA)- ketonic M^{+n} complexes: (Na^+, Li^+, K^+, Be^{++}, Mg^{++}, and Ca^{++}) cations in N_9 and O_{12} site at the B3LYP/6-31G(d) level indicate that the complexation structure is clearly located on the oxygen atom O_{12} by the small distance O_{12}--- M^{+n} compared to that of N_9---M^{+n}. The distances between metal cations and the coordinating site of (UA)-Keto in the complexes are 1,72 (Li^+), 2,08 (Na^+), 2,46 (K^+), 1,38 (Be^{++}), 1,86 (Mg^{++}), 1,86 (Ca^{++}). And are clearly shown in **Figure 7.**

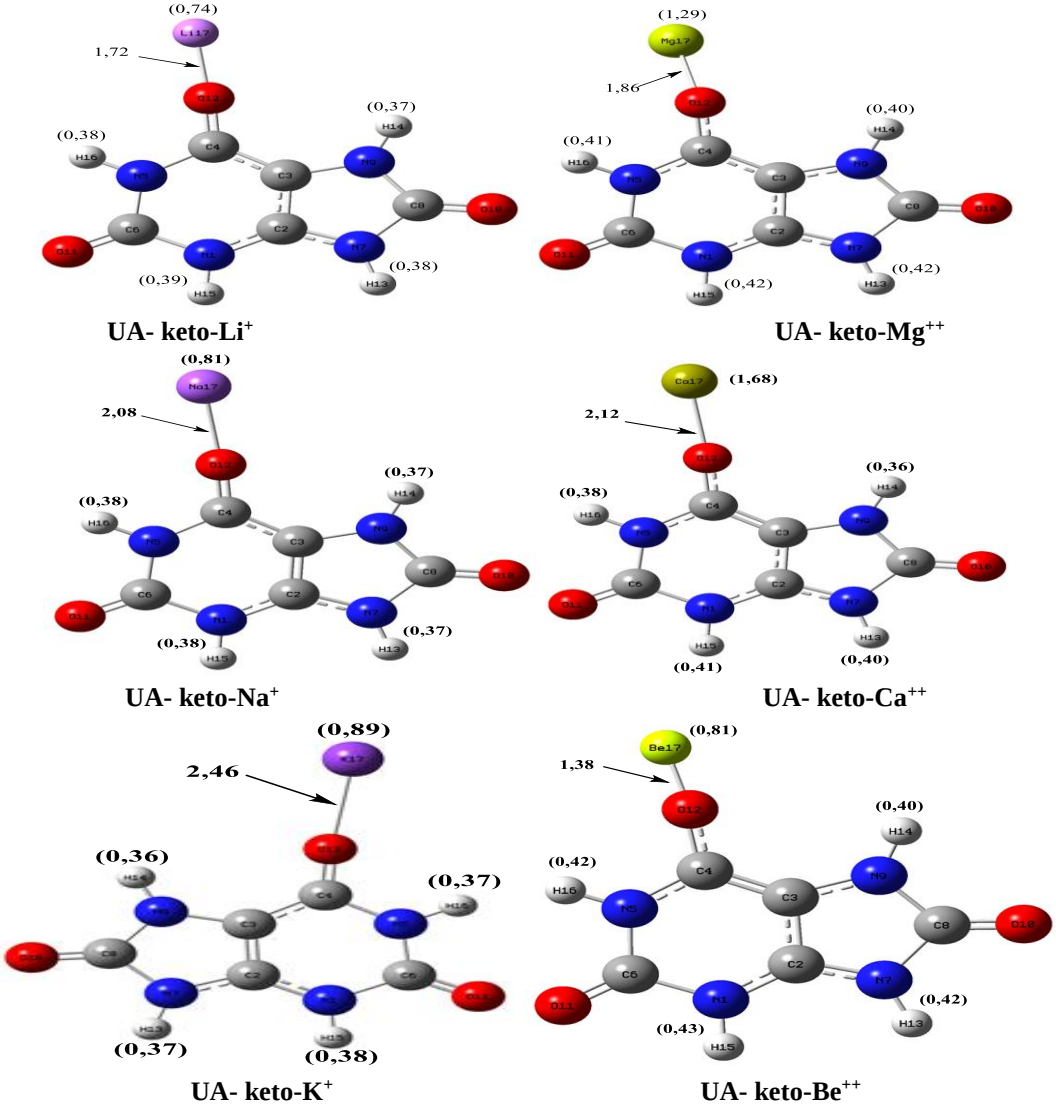

UA- keto-Li^+ **UA- keto-Mg^{++}**

UA- keto-Na^+ **UA- keto-Ca^{++}**

UA- keto-K^+ **UA- keto-Be^{++}**

Figure 7. Structures of alkali metal complexes of UA-keto form

3.4.1. IR vibration for alkali metal complexes of UA-keto form

We have taken UA-Keto form as a reference to compare the values of IR frequencies of all UA-Keto-metal complexes form. Consequently, all frequencies of stretching bond have lower values than those of UA-Keto. In addition, the site in which complexation is made, frequency of C_4=O_{12} bonds are obviously reduced for **Li^+**, **Na^+** and **K^+**. In the case of the complexation of UA-keto with divalent metal cation **Be^{++}, Ca^{++}, Mg^{++},** there is no frequency associated with the stretching of the C_4=O_{12} bond. This frequency is removed from the infrared spectrum by complexation effect. In the following discussion, the uric acid, pyrimidine and imidazole rings are designated as RingI and RingII respectively (Figure.1.).

B3LYP calculations give N-H stretching modes of the imidazole ring in the range 3662-3682 cm^{-1} and the bands are observed in gas phase and in water at 3667 ,3677,3678, 3880 cm^{-1} in the IR spectrum. The pyrimidine ring has three stretching modes tow of N-H stretching and one for C=O stretching.

Monovalent cations were shown to have a little decline on N-H and C=O stretching vibrational frequencies. However, divalent cations generate a significant decrease when compared to free UA-keto. A significant red-shift in the N-H vibration compared to that in the UA-keto is revealed for complexes of UA-keto with alkaline metal cations (Be^{++}, Mg^{++}, and Ca^{++}).

Additionally, in alkaline metal complexes, the vibration C4=O12 has disappeared on the spectrum due to the complexation effect.

In gas phase, only the complexation with calcium cation manifests as transition states by the presence of an imaginary frequency ν = -27,34 cm^{-1} that corresponds to the deformation out of the plane of N9-H14. In water environment, free UA-keto is the only one stable structure. However, all the other UA-keto metal complexes are maxima with an imaginary frequency that matches the deformation out of the plane of O12----M^{+n} bonds. **Table 3.**

Table 3. shows the computed (scaled wavenumbers), observed IR bands, and assignments for UA-keto and its metal complexes.

Stretching Bonds (Cm^{-1})	**UA-keto**	**UA- keto-K^+**	**UA- keto Li^+**	**UA- keto Na^+**	**UA- keto Be^{++}**	**UA- keto Ca^{++}**	**UA-keto Mg^{++}**
νN_9-H_{14}	3680,82	3691,14	3682,70	3688,11	3631,26	3688,65	3638,11
νN_9-$H_{14(water)}$	3678,81	3692,45	3681,22	3685,53	3632,22	3688,87	3636,41
νN_1-H_{15}	3641,02	3612,63	3600,40	3607,29	3524,94	3567,24	3540,23
νN_1-$H_{15(water)}$	3643,66	3621,75	3596,59	3603,49	3530,47	3559,03	3547,11
νN_5-H_{16}	3607,27	3607,82	3599,49	3604,43	3561,20	3607,56	3572,43
νN_5-$H_{16(water)}$	3604,13	3607,62	3699,07	3601,99	3564,16	3608,09	3573,42
νN_7-H_{13}	3667,42	3645,45	3636,09	3641,61	3566,21	3604,78	3579,34
νN_7-$H_{13(water)}$	3677,34	3646,37	3629,33	3643,75	3559,17	3598,24	3579,05
νC_8=O_{10}	1876,64	1901,99	1913,28	1906,91	1935,97	1933,73	1918,82
νC_8=$O_{10(water)}$	1858,81	1889,93	1903,00	1959,62	1959,62	1932,23	1950,02
νC_6=O_{11}	1838,18	1863,12	1874,06	1868,05	1904,37	1893,38	1896,00
νC_6=$O_{11(water)}$	1816,95	1846,92	1859,28	1914,61	1914,61	1885,35	1906,08
νC_4=O_{12}	1807,83	1733,85	1718,91	1724,90	---------	--------	---------
νC_4=$O_{12(water)}$	1783,40	1692,33	1683,06	1683,10	---------	--------	---------
Imaginary frequency (water)	does not exist	-30,60: Deformation in the plane of O_{12}----K^+	-136,56: Deformation in the plane of O_{12}----Li^+	-52,67: Deformation out of the plane of O_{12}----Na^+	-243,90: Deformation out of the plane of O_{12}----Be^{++}	-127,18 Deformation out of the plane of O_{12}----Ca^{++}	-106,56 Deformation out of the plane of O_{12}----Mg^{++}
Imaginary frequency (g)	does not exist	does not exist	does not exist	does not exist	does not exist	-27,34: Deformation out of the plane of N9-H14	does not exist

The energetic gaps $\Delta E_{HOMO-LUMO}$ in free UA-keto are almost equal in gas phase and in water, this is also remarkable in the case of monovalent metal complexes. However, for divalent metal complexes there is a measurable distinction. In this case higher or lower energy of HOMO and LUMO by metal complexation is referred to free UA-keto molecule. Furthermore, UA-Keto-Be^{++} and UA-Keto-Mg^{++} in gas phase seems to be more reactive according to the lowest gap value **Table 4.** This difference reflects a significant charge transfer this therefore makes these species more reactive.

Each of the proton in UA-Keto form links to an atom of nitrogen, H16 is more acidic because of its location between two carbonyl functions and as stated by NMR $_1{}^1H$ chemical shift value **Table 4.** whereas in UA-Keto metal Complexes, H15 seems to be the most acidic proton. Subsequently, UA-Keto-Be^{++} shows the highest value of δ (8,15 and 8,10 ppm in gas phase and in water respectively)

which is in good agreement with the deprotonation energy values.

3.5. Complexation of Uric Acid [M(UA)] $^{+n}$ in its enolic form

Uric Acid coordinates different alkali metals ions through the interaction of N9 atom within the imidazole ring and O12 atom within the pyrimidine ring. These two atoms carry more electronegative charge confirming active sites for coordination, and consequently the obtained complex, after geometry optimization calculations, reveals a pseudo five-membered ring in which the metal cation prefers to be coordinate with the nitrogen atom compared to the oxygen atom. This is clearly apparent in all complexes.

Table 4. δ $_1$[1]H chemical shift(ppm), deprotonation energy DE (Kcal/mol), ΔE $_{HOMO-LUMO}$ (eV) Gap and dipolar moment μ_{Total} (Deby) of studied complexes in gas phase and in water.

Complexes	δH13	δH14	δH15	δH16	DE	ΔE	HOMO	LUMO	μ_{Total}
UA-Keto(g)	4,79	4,95	5,00	**6,23**	496.99	5.068	-5.909	-0.912	3.047
UA-Keto(water)	6,40	6,01	6,63	**6,47**	284.26	4.993	-5.733	-0.740	4.244
UA-Keto-Li^+(g)	5,69	4,91	**6,15**	5,98	703.44	4.366	-9.546	-5.180	10,885
UA-Keto-Li^+(water)	6,78	6,21	**7,16**	7,05	295.56	4.719	-6.074	-1.355	13,062
UA-Keto-Na^+(g)	5,55	4,79	**5,97**	5,79	693.40	3.836	-9.179	-5.343	12,039
UA-Keto-Na^+(water)	6,67	6,14	**7,00**	6,89	298.07	4.799	-5.956	-1.157	13,922
UA-Keto-K^+(g)	6,14	5,42	**6,53**	6,33	685.24	4.072	-8.892	-4.820	12,731
UA-Keto-K^+(water)	6,59	6,10	**6,90**	6,77	564.13	4.851	-5.890	-1.040	14,354
UA-Keto-Be^{++}(g)	7,68	7,06	**8,15**	6,86	827.69	0.700	-14.395	-13.695	14,698
UA-Keto-Be^{++}(water)	7,60	6,66	**8,10**	7,60	596.76	4.296	-6.813	-2.517	23,085
UA-Keto-Mg^{++}(g)	6,77	5,91	**7,24**	6,33	800.08	0.893	-13.719	-12.826	16,019
UA-Keto-Mg^{++}(water)	7,20	6,43	**7,65**	7,33	576.05	4.443	-6.245	-1.802	27,605
UA-Keto-Ca^{++}(g)	6,32	4,69	**6,79**	5,67	778.74	1.112	-12.443	-11.331	23,852
UA-Keto-Ca^{++}(water)	6,97	6,23	**7,36**	7,15	574.80	4.635	-6.194	-1.560	28,886

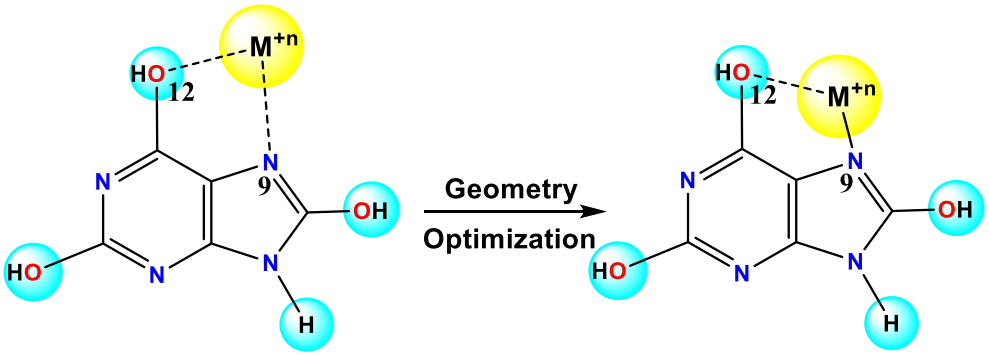

Figure 8. metal complexation of Uric acid in its enolic form

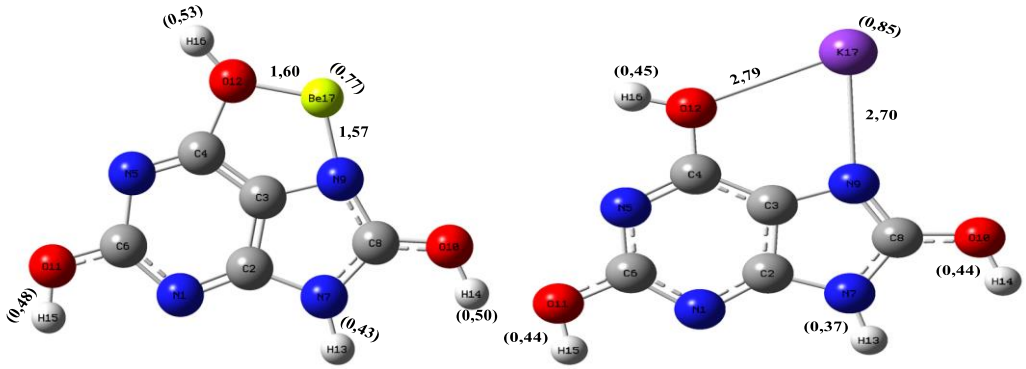

UA-enol-Be^{++} **UA-enol-K^+**

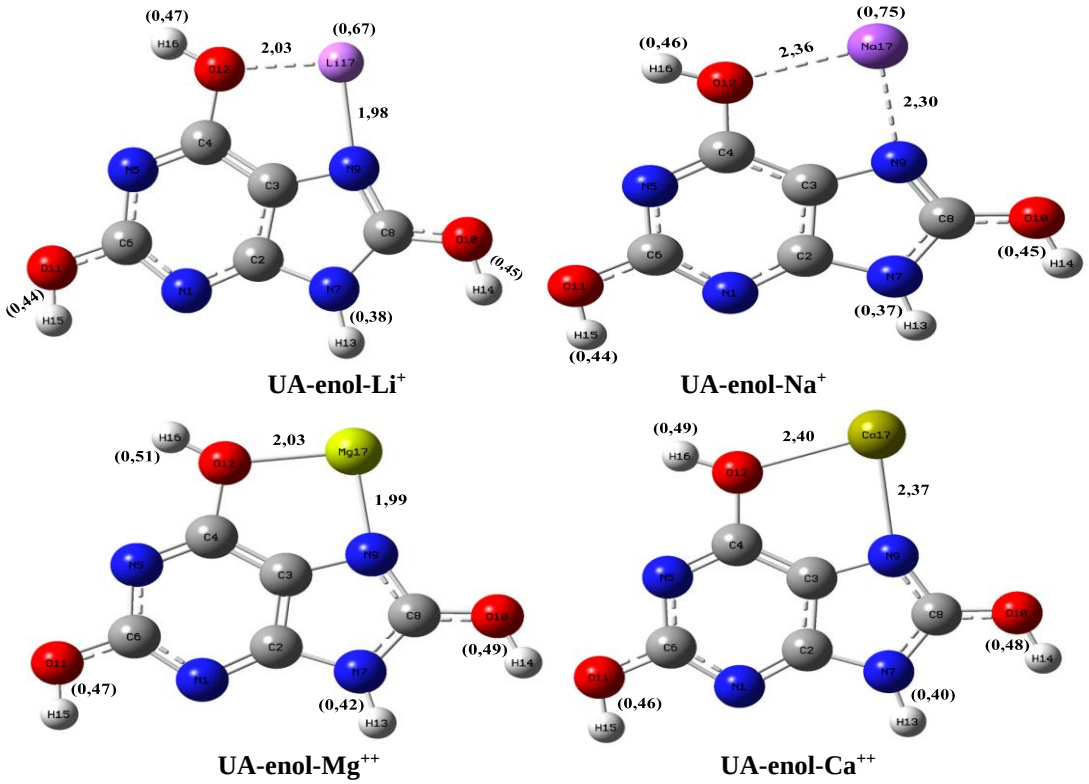

Figure 9. Optimized structures of alkali metal complexes of UA-enol form

Table 5. Observed IR bands, and assignments for UA-enol and its metal complexes.

Stretching Bonds	**UA-enol**	**UA-enol-K^+**	**UA-enol-Li^+**	**UA-enol-Na^+**	**UA-enol-Be^{++}**	**UA-enol-Mg^{++}**	**UA-enol-Ca^{++}**
νO_{10}-$H_{14(g)}$ νO_{10}-$H_{14(water)}$	3771,98 3781,28	3756,42 3756,44	3748,28 3752,04	3752,80 3759,04	3760,15 3759,80	3692,15 3676,57	3712,29 3708,44
νO_{11}-$H_{15(g)}$ νO_{11}-$H_{15(water)}$	3726,61 3730,12	3717,73 3713,84	3713,18 3709,85	3715,78 3712,64	3721,67 3713,69	3679,69 3670,72	3691,12 3683,23
νO_{12}-$H_{16(g)}$ νO_{12}-$H_{16(water)}$	3685,20 3687,31	3664,41 3667,93	3672,55 3673,84	3665,51 3667,81	3666,85 3673,52	3585,50 3594,40	3605,33 3614,53
νN_7-$H_{13(g)}$ νN_7-$H_{13(water)}$	3641,40 3654,62	3627,56 3632,23	3621,02 3627,58	3624,91 3631,38	3628,40 3638,12	3573,27 3573,23	3589,13 3589,14
Imaginary frequency (g)	-118,26 : Deformation out of the plane O10-H14	Does not exist	Does not exist	Does not exist	-311,97: Deformation out of the plane O12-H16	Does not exist	Does not exist
Imaginary frequency (w)	-186,01 : Deformation out of the plane O10-H14	-35,17: Deformation out of the plane of K^+	-216,53: Deformation out of the plane of N9---Li^+	-62,19: Deformation out of the plane of Na^+	-241,51: Deformation out of the plane O12-H16	-157,48: Deformation out of the plane of Mg^{++}	-88,48: Deformation out of the plane of Ca^{++}

UA-enol-complexes reduce IR frequency values as compared to isolated UA-enol structure. The IR frequencies of the O-H and N-H bonds are reduced by UA-enol-complexation. The results show that complexation with divalent metal cation generates a substantial decrease in IR frequencies when compared to monovalent metal complexes. In addition, for the complexes of monovalent metal cations, the IR frequencies of each O-H or N-H bond rise in the solvated phase relative to the gas state; however, no change is shown in the case of UA-enol-K+. This frequency does, however, reduces for divalent metal cation complexes, with UA-enol-Be++ showing a minor variation. O-H and N-H bond IR frequencies may generally be attenuated by complexation, either by monovalent

or divalent metal cations, in comparison to the identical bonds in the UA-enol free structure.

UA-enol already has an imaginary frequency in gas phase and in water. Therefore, in gas phase complexation with metal cations was able to improve the structure in order to create a more stable systems (UA-enol-K+, UA-enol-Li+, UA-enol-Na+, UA-enol-Mg++, UA-enol-Ca++) as seen in **Table 5.** In water, all metal complexes are maxima presenting one imaginary frequency.

3.5.1. NMR $_1{}^1$H Chemical Shift of UA-enol and its complexation

Principally in the enolic form of UA, the proton H13 remains bonded to nitrogen atom, and all the other protons are bonded to oxygen atoms.

The proton H13 appears to be the most acidic in the enolic form and its complexes. This is supported by the $\delta^1{}_1$H NMR chemical shift (ppm) and deprotonation energy DE (Kcal/mol) results. **Table 6.**

Table 6. Chemical shifts $\delta\ ^1{}_1$H (ppm) of the different protons in UA-enol form, DE(Kcal/mol, $\Delta E_{(HOMO\text{-}LUMO)}$ (eV), μ_{Total} (Deby).

Complexes	δH_{14}	δH_{15}	δH_{16}	δH_{13}	ΔE	HOMO	LUMO	DE	μ_{Total}
UA-enol$_{(g)}$	4,07	5,36	5,65	**6,49**	5.447	-5.860	-0.412	621.71	5,21
UAenol-$_{(w)}$	5,48	5,94	6,03	**7,50**	5.434	-5.995	-0.561	581.12	6,77
UA-enol-$K^+{}_{(g)}$	5,32	6,38	5,80	**7,14**	4.97	-9.33	-4.36	--------	08,88
UA-enol-$K^+{}_{(w)}$	5,98	6,25	6,04	**6,64**	5.42	-6.24	-0.82	300.10	10,75
UA-enol-$Li^+{}_{(g)}$	5,89	6,75	6,31	**7,32**	5.33	-10.00	-4.67	---------	06,83
UA-enol-$Li^+{}_{(w)}$	6,40	6,49	6,40	**7,76**	5.40	-6.46	-1.06	296.85	08,91
UA-enol-$Na^+{}_{(g)}$	5,60	6,55	6,02	**7,24**	4.93	-9.68	-4.75	---------	07,71
UA-enol-$Na^+{}_{(w)}$	6,18	6,34	6,18	**7,69**	5.41	-6.34	-0.93	286.81	12,76
UA-enol-$Be^{++}{}_{(g)}$	**7,99**	**8,23**	**8,61**	**8,88**	3.16	-14.92	-11.76	---------	09,68
UA-enol-$Be^{++}{}_{(w)}$	**7,67**	**7,10**	**7,89**	**8,72**	5.20	-7.57	-2.37	262.56	16,18
UA-enol-$Mg^{++}{}_{(g)}$	7,57	8,16	7,22	**8,28**	2.76	-14.06	-11.30	---------	12,73
UA-enol-$Mg^{++}{}_{(w)}$	7,35	7,12	7,12	**8,13**	5.38	-7.00	-1.62	287.29	17,41
UA-enol-$Ca^{++}{}_{(g)}$	6,95	7,74	6,58	**8,04**	2.03	-13.31	-11.28	---------	15,53
UA-enol-$Ca^{++}{}_{(w)}$	6,79	6,79	6,53	**7,95**	5.34	-6.66	-1.32	293.17	20,14

We employed δ NMR ^{1}H chemical shift as a tool to measure and evaluate acidity of all protons which at significant δ NMR ^{1}H values generate the maximum acidity. Consequently, the proton H13 seems to be more acidic according to the chemical shift values **Table 6.** Particularly these values influence the divalent metals complex (Be++, Mg++ and Ca++) and more special affect the case of complexation with Be++.

Generally, and for all structure $\Delta E_{HOMO\text{-}LUMO}$ gap is relatively higher in the case of water effect than the gas phase. Additionally, the complexes with monovalent metals are more stable than those with divalent metal and consequently the lowest gap $\Delta E_{HOMO\text{-}LUMO}$ appears in UA-enol-Mg^{++} and UA-enol-Ca^{++}.

3.6. Metal Complexes of Uric Acid $[M(UA)_2]^{+n}$ in its ketonic form

Uric Acid (UA) has also the ability to generate strong complexes with many different transition metal cations, including Zn^{2+}, Cd^{2+}, Cu^+ and Ag^+

Figure 10. Acid dissociation constants are related to the metal interaction affinities of these functional groups (N-Metal-N) and are therefore important for investigating the deprotonation in aquatic systems. In the current study, we used GIAO-NMR $_1{}^1$H chemical shift together with deprotonation energy (DE) in the (PCM) solvent model for estimating the proton acidity in different complexes.

Olga et al. **[24]** have been studied a series of metal uric acid complexes. These complexes were synthesized using different ions of Zn^{+2}, Cd^{+2}, Cu^+ and Ag^+ in aqueous solution. Experimental results indicate that IR spectrum exhibits three different C=O absorption bands. The 1701 and 1671 cm^{-1} bands are due to the carbonyl of the pyrimidine ring, and the third at 1655 cm^{-1}corrsponds to the carbonyl of the imidazole ring. The same bands are calculated in water for (UA) in its ketonic form and the frequencies are: tow frequencies C=O 1816,95 cm^{-1}, 1783,40 cm^{-1} for pyrimidine ring and 1858,81 cm^{-1} for C=O of the imidazole ring. Obtained UA-metal complex structures were explored on the

basis of Density Functional Theory calculations using B3LYP/6-31G(d,p) and LANL2DZ for Ag, Zn, Cd, Cu atoms. The acidity prediction was estimating for each complex by calculating the deprotonation energies and NMR $^{1}{}_{1}H$ δ (ppm) chemical shift. Therefore, experimental IR spectrum **Table 7.** shows for all the complexes except Cd^{+2} a shift from 1671 to 1609 cm^{-1} of the carbonyl of the pyrimidine ring.

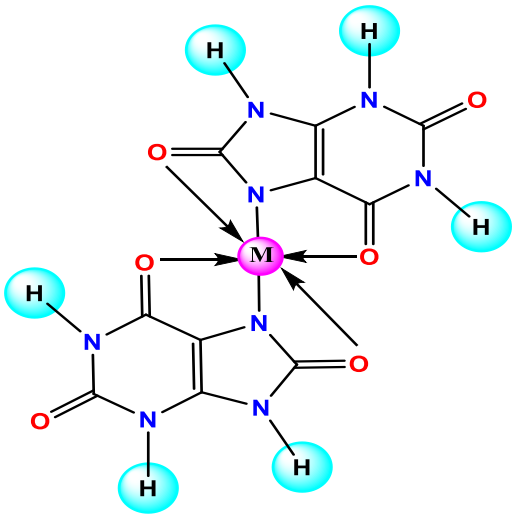

Figure 10. (UA) transition complexation in ketonic form

3.6.1. IR vibration of Keto-metal complexes $[M(UA)_2]^{+n}$

Table 7. experimental and calculating C=O frequencies of triketo-forme of UA and its metal complexes.

Complexes	C8=O10 imidazole ring	C4=O12 pyrimidine ring	C6=O11 pyrimidine ring	N-H13	N-H14	N-H15
UA-Keto/(exp)[24]	1858,81 (1655)	1783,40 (1671)	1816,95 (1701)	3677,34	3643,66	3604,13
$[Ag(UA)_2]^{+}$	1679,08	1653,15	1696,56	3654,19	3591,40	3589,29
$[Zn(UA)_2]^{+2}$	1680,99	1690,00	1639,46	3628,56	3583,39	3579,48
$[Cd(UA)_2]^{+2}$	1663,96	1653,48	1695,19	3632,62	3598,50	3590,51
$[Cu(UA)_2]^{+}$	1681,98	1657,60	1688,01	3647,33	3597,66	3695,49

Table 8. δ NMR $^{1}{}_{1}H$ (ppm) Chemical shifts of the different protons, deprotonation energy DE (Kcal/mol), HOMO-LUMO gaps $\Delta E_{HOMO-LUMO}$ (eV) and dipolar moment μ_{Total} (Deby)of different complexes

Complexes	δ H_{13}	δ H_{14}	δ H_{15}	DE	ΔE	HOMO	LUMO	μ_{Total}	N-M-N (°)
$Ag(UA)_2^{+}$	7,09	7,30	**7,30**	294.89	0.65	-6.188	-5.538	0.876	177,93
$Zn(UA)_2^{+}$	7,28	7,61	**7,69**	**285.99**	0.49	-6.505	-6.018	2,008	150,69
$Cd(UA)_2^{+2}$	7,29	7,66	**7,77**	292.91	0.46	-6.226	-5.767	1,226	139,98
$Cu(UA)_2^{+}$	7,04	7,28	**7,33**	295.07	0.78	-6.335	-5.559	6,045	170,80

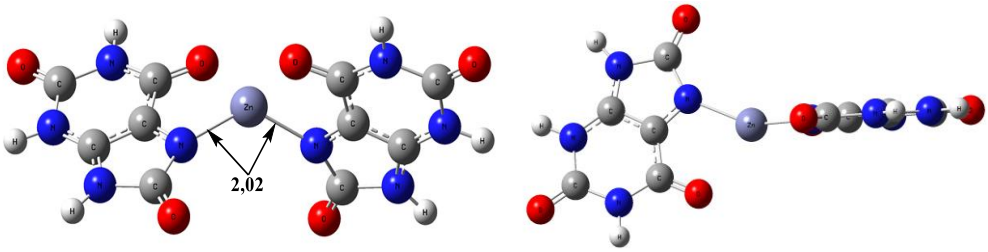

Figure 11. $Zn(UA)_2^{++}$ complex

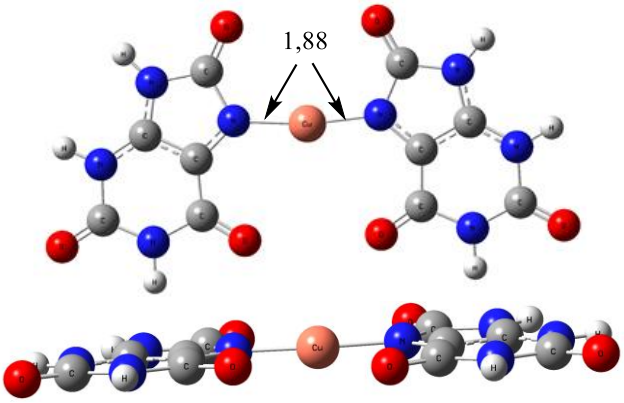

Figure 12. $Cu(UA)_2^{+}$ complex

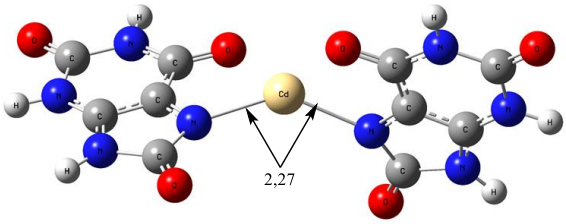

Figure 13. $Cd(UA)_2^{++}$ complex

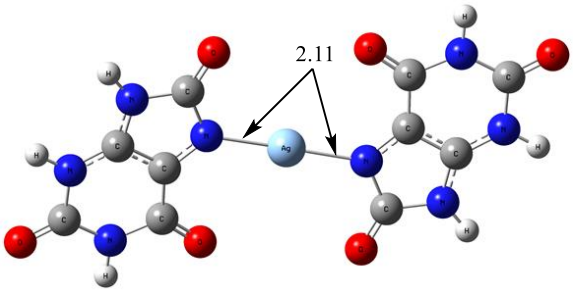

Figure 14. $Ag(UA)_2^{+}$ complex

3.6.2. Structure and acidity of $[M(UA)_2]^{+n}$ metal complexes

All optimized geometries of metal complex are shown in **Figure. 11, 12, 13** and **14.** According to **Table 8.** The acidity of the different protons estimated by Chemical shifts $^1{}_1H$ δ (ppm) values indicates that H15 seems to be the most acidic proton. Consequently, only for the most acidic protons, which is estimated by δ NMR $^1{}_1H$ (ppm) Chemical shifts, deprotonation energy is calculated. All complexes are optimized and shown in **figures: 11., 12., 13** and 14. As a starting point, we have analysed the structure and the electronic charge distribution in order to investigate the lone pairs interactions of oxygen and/or nitrogen atoms with the studied complexes $Ag(UA)_2^{+}$, $Zn(UA)_2^{+2}$, $Cu(UA)_2^{+}$, $Cd(UA)_2^{+2}$.

3.7. Metal complexation of uric acid $[M(UA)_2]^{+n}$ in the enolic form

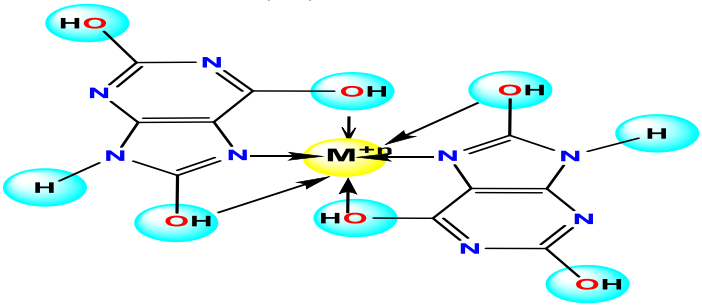

Figure 15. complexation of (UA) with transition metals

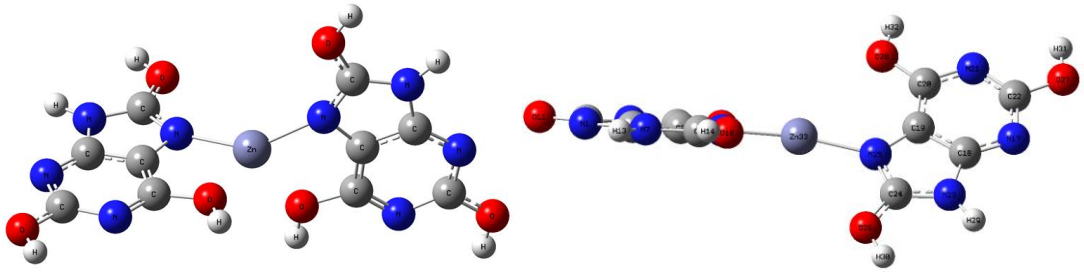

Figure 16. optimised geometry of **(UA)$_2$enol-Zn^{+2}**

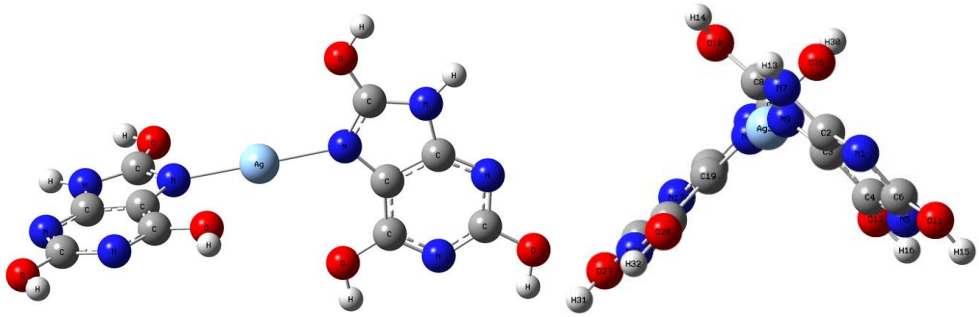

Figure 17. optimised geometry of **(UA)2enol-Ag** $^{+}$complex

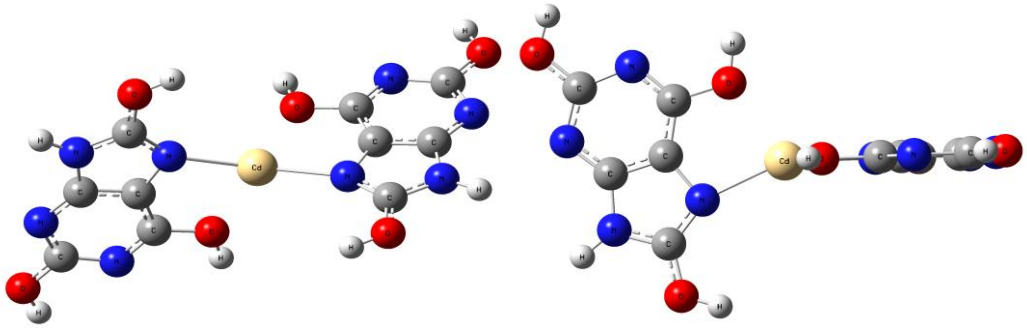

Figure 18. optimised geometry of **(UA)2enol-Cd^{++}**

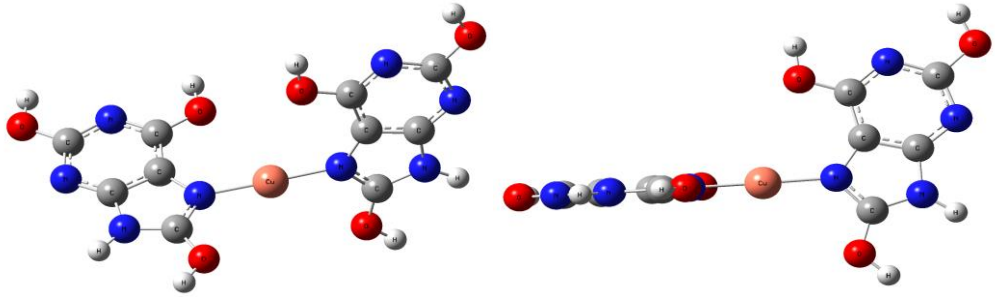

Figure 19. optimised geometry of **(UA)2enol-Cu^{+}**

Table 9. IR vibration frequencies of O-H and N-H stretching (cm$^{-1)}$ metal-N distance (Å) and N-M-N angle (°) in enol-complexes.

Complexes	O10-H14 imidazole ring	O11-H15 pyrimidine ring	O12-H16 pyrimidine ring	N7-H13	metal-N	N-M-N
UA-enol	3781,28	3730,12	3687,31	3654,62	-------	--------
$[Ag(UA)_2]^+$	3710,47	3679,66	3655,33	3642,88	2,13	179,35
$[Zn(UA)_2]^{+2}$	3689,04	3675,45	3655,48	3649,51	2,02	162,11
$[Cd(UA)_2]^{+2}$	3705,68	3679,71	3654,04	**3657,51**	2,30	161,51
$[Cu(UA)_2]^+$	3697,48	3679,40	3652,86	3648,70	1,90	179,23

Table 10. δ $^{1}{}_{1}$H (ppm), DE(Kcal/mol), $\Delta E_{HOMO\text{-}LUMO}$ (eV) and μ_{Total} (Deby), DE(Kcal/mol)

Complexes	δ H14	δ H15	δ H16	δ H13	DE	ΔE	HOMO	LUMO	μ_{Total}
$Ag(UA)_2^+$	6,19	6,08	5,81	**7,37**	292.11	5.30	-6.975	-1.673	5,341
$Zn(UA)_2^{+2}$	6,63	6,12	6,12	**7,60**	224.09	5.32	-7.241	-1.925	9,188
$Cd(UA)_2^{+2}$	6,73	6,55	5,83	**7,63**	**89.17**	5.36	-7.263	-1.903	1,861
$Cu(UA)_2^+$	6,37	6,00	5,92	**7,36**	290.26	5,05	-6.823	-1.775	6,594

Table 11. Second-order perturbation theory of the Fock matrix in the NBO basis for (UA)2Ag+, (UA)2Zn+2, (UA)2Cd+2, (UA)2Cu+ complexes.

Complexes	Donor (i)	Donor occupation	Acceptor (j)	Acceptor occupation	$E^{(2)}$ (Kcal/mol)
$(UA)_2Ag^+$	LP(N9)	1.81628	LP*(Ag)	0.26300	44.68
	LP(N25)	1.81628	LP*(Ag)	0.26300	44,67
	LP(N7)	1.61401	BD* C8-N9	0.44241	61.61
$(UA)_2Zn^{+2}$	LP(N9)	1.86666	LP*(Zn)	0.17994	37.77
	LP(N25)	1.86678	LP*(Zn)	0.17994	38.02
	Lp(N7)	1.60268	BD* C8-N9	0.46450	68.17
$(UA)_2Cd^{+2}$	LP(N7)	1.60172	BD* C8-N9	0.44619	65.74
	LP2(O10)	1.84055	BD* C8-N9	0.44619	46.44
	LP(N9)	1.88443	LP*(Cd)	0.13612	16.65
	LP(N25)	1.88443	LP*(Cd)	0.13612	16.65
$(UA)_2Cu^+$	LP(N9)	1.80083	LP*(Cu)	0.29054	66.82
	LP(N25)	1.80083	LP*(Cu)	0.29054	66.82
	LP(N7)	1.60741	BD* C8-N9	0.45844	64.45
	LP(O10)	1.84095	BD* C8-N9	0.45844	45.65

$E^{(2)}$ refers energy of interaction.

The vibrational modes of O-H stretching of all $[M(UA)_2]^{+n}$ complexes are thought to be lower than the frequency of UA-enol without any complexation. N7-H13 stretching mode is observed for UA-enol at 3654,62 cm^{-1}. However, with the exception of $[Cd(UA)_2]^{+2}$, which has a greater value, all complexes have this frequency attenuated.

In the pyrimidine ring, the stretching vibrations, O11-H15 and O12-H16, in different complexes have a range of close values. However, in the case of imidazole ring, a slight difference frequency appears in stretching vibration O10-H14.

The distance that separates the metal ion **Table 9.** from the two ligands seems to be the lowest in $[Zn(UA)_2]^{+2}$ The event that it is in the order $Cd(UA)_2^{+2} > Ag(UA)_2^{+} > Zn(UA)_2^{+2} > Cu(UA)_2^{+}$.

$\Delta E_{HOMO\text{-}LUMO}$ gap is in the order $Cd(UA)_2^{+2} > Zn(UA)_2^{+2} > Ag(UA)_2^{+} > Cu(UA)_2^{+}$.

The three parameters (δ ^{1}H chemical shift, *ν*(N–H13) vibration and deprotonation energy DE) adopt the same variation in complexes **Table 10.**

3.7.1. Natural Bond Orbital (NBO) Analysis and Charge Distribution.

A practical foundation for examining charge transfer or conjugative interaction in molecular systems is provided by natural bond orbital analysis. Several electron orbitals that are donor, acceptor, and the second-order perturbation of the Fock matrix were used to evaluate the impact of coordination and electron distribution on the ligands and metal d-orbitals.

As in our previous work **[38,39]**, A useful foundation for examining charge transfer or conjugative interaction in molecular systems is provided by natural bond orbital analysis. **Table 11.** lists the major interactions in the calculated complex structures.

In the case of $(UA)_2Ag^+$ the occupancy of LP(N9) and LP(N25) is (1.81628), these two lone pairs act as donor in intramolecular interactions to LP*(Ag): LP(N9) → LP*(Ag), LP(N25) → LP*(Ag) with interaction energy of (44,68 Kcal/mol). Thus, intramolecular interaction from LP(N7) to BD* C8-N9 leading to stabilization energy of (61,61 kcal/mole).

On this particular case of $(UA)_2Cd^{+2}$ we notice that a strong intramolecular interaction in the pyrimidine ring from BD* C20-N21 to BD* C18-C19 with stabilization energy 121,20 kcal/mol. However, the same interaction in $(UA)_2Ag^+$, $(UA)_2Cu^+$ gave only (9,18), (9,44) and (9,47) kcal/mol respectively. In the imidazole ring, the

interactions from LP(N7) to BD* C8-N9 have comparable values in all complexes.

Besides, transition monovalent metal cation charges (Ag+ and Cu+) seems to be higher in the case of the ketonic complexes compared to the enolic complexes. Consequently, the metal cation's electronic charge is more provided by the enolic complex than the ketonic. Thus, we note that the positive charge labelled Zn++ and Cd++ is higher in the case of enolic complexes. In this case the ketonic complex provided more electronic charge to the metal center. Atomic charges of metal complexes are listed in **Table 12.**

For the other atoms we note that, for the other atoms we notice that, in enol complexes, the heteroatoms (N9, O10, O12) gave more electronic density and appear with weaker negative charges. C4 and C8 atoms appear as very poor in electronic density with a large positive charge, while C3 atom is indicated by weak positive charge. These findings relate to both forms of complexes.

Table 12. NPA atomic charge distributions of some selected atoms in the enol-complexes. values in parentheses are for keton-complexes

Charges				
Atom and	$(UA)_2Ag^+$	$(UA)_2Zn^{+2}$	$(UA)_2Cd^{+2}$	$(UA)_2Cu^+$
N9	-0.67 (-0.63)	-0.76 (-0,69)	-0.73 (-0,70)	-0,68 (-0,67)
O10	-0.71 (-0,58)	-0,70 (-0,56)	-0.70 (-0,46)	-0,70 (-0,58)
O12	-0,71 (-0.60)	-0,71 (-0.64)	-0.71 (-0,68)	-0,71 (-0,61)
C3	0,03 (0.10)	0.03 (0,12)	0.03 (0.09)	0,03 (0,10)
C4	1,61 (0.68)	0.62 (0,68)	1,61 (0,68)	0,61 (0.67)
C8	0,84 (0,85)	0,85 (0,85)	0.83 (0,84)	0,84 (0,89)
Ag^+	0,71 (0,76)	------	------	------
Zn^{+2}	------	1,76 (1,67)	------	------
Cd^{+2}	------	------	1,82 (1,57)	------
Cu^+	------	------	------	0,67(0,82)

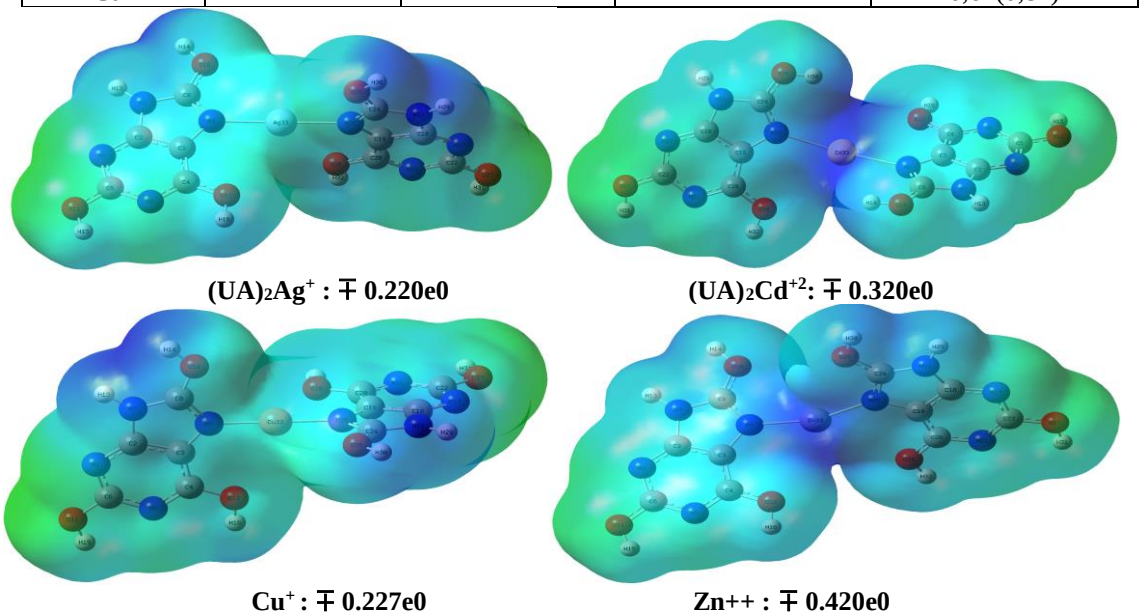

$(UA)_2Ag^+$: ∓ 0.220e0 **$(UA)_2Cd^{+2}$: ∓ 0.320e0**

Cu^+ : ∓ 0.227e0 **Zn++ : ∓ 0.420e0**

Figure 20. Electrostatic surface potential map of metal complexes

3.7.2. Molecular Electrostatic Potential Surface (MEPS)

A useful tool for understanding and forecasting molecular behaviour is the molecular electrostatic potential surface (MEPS) map. MEPS map provides a visual method to understand the relative polarity of the molecule, predict the reactive site of the molecule and illustrates the charge distribution three dimensionally. It is primarily used to study the reactivity towards

electrophilic and nucleophilic attack as well as hydrogen bonding interactions.

In the electrostatic potential map **Figure 20.** The total density depicts the localization of charges surrounding the atoms; it should be noticed that the richness of electrons is concentrated in the red, green and yellow color regions, the blue region of EPS relates to the positive charge.

The largest interval of electron density has been found for $(UA)_2Zn^{+2}$ complex and it tends to be between ∓ 0.420e0. However, the restraint interval of electron density characterizes $(UA)_2Ag^{+}$complex and it tends toward ∓ 0.220e0. **Figure 20.**

3.7.3. Energy and Relative Stability of Complexes

As a result, we have calculated the difference total energy ΔE(eV) between alkali metal complexes and transition metal complexes in their ketonic and enolic forms **Table 13.** Generally, the following results (**Table 13.**) show that in the ketonic form, alkali metal complexes are more stable than the same complexes in the enolic form. ΔE indicates a margin that reflects which the more most stable complex in ketonic form by the large energy value shown. The range of values ΔE is relatively wide and we can present the more stable alkali metal complexes in the following order , (UA)-Be^{++} is more stable (1.73 eV).

Ketonic form (alkali metal complexes): (UA)-Be^{++} > (UA)-Mg^{++} > (UA)-Li^{+} > (UA)-Ca^{++} > (UA)-Na^{+} > (UA)-K^{+}.

On the other hand, the enolic form is obviously more stable than the ketonic form in the event of transitions metal complexes. The range of values ΔE in this case is more restricted and the order is in following.

Ketonic form (transition metal complexes): (UA)2-Cu^{+} > (UA)2-Zn^{++} > (UA)2-Cd^{++} > (UA)2-Ag^{+}

(UA)2-Cu^{+} is evidently with greater stability (33,03 eV).

Ketonic form adopts the alkali metal complexes notably the divalent cations. However, the enolic form attracts transition metals better to stabilise their complexes.

Table 13. total energy and their difference ΔE(eV) between alkali metal complexes and transition metal complexes of ketonic and enolic (UA) forms.

Complexes	Enolic form (Hartree)	Ketonic form (Hartree)	ΔE(eV)
Alkali Metal Complexes			
(UA)-Li^{+}	-645,132517	-645,184750	1,42
(UA)-Na^{+}	-799,899074	-799,946109	1,28
(UA)-K^{+}	-1237,508151	-1237,553431	1,23
(UA)-Mg^{++}	-837,526320	-837,582202	1,52
(UA)-Be^{++}	-652,078829	-652,142283	1,73
(UA)-Ca^{++}	-1315,078552	-1315,127788	1,34
Transition Metal Complexes			
(UA)2-Ag^{+}	-1420,768294	-1419,586739	32,15
(UA)2-Cu^{+}	-1471,171029	-1469,957092	33,03
(UA)2-Zn^{++}	-1340,471568	-1339,268485	32,74
(UA)2-Cd^{++}	-1322,954782	-1321,759775	32,52

4. Conclusions

In light of the research, this study has achieved the following goals:

- (UA) has a crucial interaction to form complexes with ions of alkali and transition metals. These complexes have various geometries and possess chemical activities more than uric acid itself.
- In this work, the influence of solvent polarity on structure, electronic properties, IR spectrum and $_1{}^1H$ NMR parameters of (UA) complex was investigated.
- The results of this theoretical study about the structure and acidity of (UA) and its alkali metal complexes have shown that in its ketonic form, the metal cation is coordinated to the oxygen atom, whereas in its enolic form, the coordination occurs through the nitrogen atom.
- The interaction of different metal cations with uric acid (UA) has been studied in order to

estimate the influence of metal cations on the acidity strength of N-H and/or O-H.

- As a result, we may conclude that proton H13 in the enolic state, the cation alkali or transition metal complex, appears as more acidic acoording to δ ^{1}H NMR chemical shift and the deprotonation energy values. However, in the ketonic state, the H15 seems to be more acidic by the same parameter values.
- The results suggest that the calculated δ ^{1}H NMR chemical shift gave a good agreement with the experimental data due to the consideration of two acidities of uric acid (UA), from where one is come from enolic form (H13) and the second is coming from the ketonic form(H13).
- Complexation of (UA) with both alkali or transition metals continues to confirm the existence of two acidities by estimating one more acidic proton in each chemical form.

Acknowledgements: The authors are grateful to Messaoudi Abdelatif, Professor at the University of Batna1, for the helpful comments which was greatly appreciated.

Foundation: the research was supported by the University of Batna1, Laboratory of chemistry of materials and living organisms: Activity-reactivity (LCMVAR), department of chemistry.

Conflicts of Interest: The authors declare no conflict of interest.

References

[1] Muhammad Bilal Khattak , Zahid Irfan Marwat , Shah Nawaz , Saqib Malik , Muhammad Nadeem , Alamzeb jadoon. ASSOCIATION OF SERUM URIC ACID WITH DIABETES MELLITUS IN DISTRICT NOWSHERA KPK. KJMS, 2020 13.

[2] Scheele C. Examen Chemicum Calculi Urinari. Opuscula. (1776);2:73.

[3] Hitchings, G. H. "Uric Acid: Chemistry and Synthesis". In Kelley, William N.; Weiner, Irwin M. (eds.). Uric Acid. Handbook of Experimental Pharmacology. 51. Springer Berlin Heidelberg, 1978 1–20. https://doi.org/10.1007/978-3-642-66867-8_1.

[4] Young-Hye Cho , Youngin Lee , Jung In Choi , Sae Rom Lee , Sang Yeoup Lee, Chapter Three - Biomarkers in metabolic syndrome, Advances in Clinical Chemistry, 111 (2022) 101-156. https://doi.org/10.1016/bs.acc.2022.07.003.

[5] T.-M. Pan, S. Mondal, Structural Properties and Sensing Characteristics of Sensing Materials Comprehensive Materials Processing, 13 (2014) 179-203. https://doi.org/10.1016/B978-0-08-096532-1.01306-6

[6] H. Bouzidi, B. Lacour, M. Daudon, Ann Biol Clin, 65 (2007) 585-92.

https://doi.org/10.1684/abc.2007.0165

[7] A. R. Izatulina , V. V. Gurzhiy , M. G. Krzhizhanovskaya , Nikita V. Chukanov and Taras L. Panikorovskii, Thermal Behavior and Phase Transition of Uric Acid and Its Dihydrate Form, the Common Biominerals Uricite and Tinnunculite, Minerals 9, 2019, 373-386. https://doi.org/10.3390/min9060373

[8] L. CarolineBenn, Pinky Dua, , Rachel Gurrell, Peter Loudon, R. Andrew Pike, Ian Storer, Ciara Vangjeli, Physiology of Hyperuricemia and Urate-Lowering Treatments, frontier in medicine, 160, (2018). https://doi.org/10.3389/fmed.2018.00160

[9] Jan Meadows, Robert C. Smith, Jeri Reeves, Uric acid protects membranes and linolenic acid from ozone-induced oxidation, Biochemical and Biophysical Research Communications.

137 (1986) 536-541. https://doi.org/10.1016/0006291X(86)91243-X

[10] Daria Pasalic, Natalija Marinkovic, Lana Feher-Turkovic, Uric acid as one of the important factors in multifactorial disorders – facts and controversies, Biochem Med (Zagreb), 2012 63–75.

https://doi.org/10.11613/bm.2012.007

[11] Samir Awadallah, Chapter Three - Protein Antioxidants in Thalassemia, Advances in Clinical Chemistry 2013, 85-128, https://doi.org/10.1016/B978-0-12-407681-5.00003-9

[12] A. Halabe, O. Sperling, Uric acid nephrolithiasis. Miner Electrolyte Metab. 20 (1994), 424–431.

[13] R. Terkeltaub, DA. Bushinsky, MA. Becker, Recent developments in our understanding of the renal basis of hyperuricemia and the development of novel antihyperuricemic therapeutics. Arthritis Research & Therapy. 8 (2006) 1-9. https://doi.org/10.1186/ar1909

[14] J. A. Kelvin DAVIES, Alex SEVANIAN, Samar F. MUAKKASSAH-KELLY, Paul HOCHSTEIN Uric acid-iron ion complexes A new aspect of the antioxidant functions of uric acid, Biochem. J. 235 (1986) 747-754. https://doi.org/10.1042/bj2350747

[15] V.Venkata Ramana, V.J. Thyagaraju, K.Sivarama Sastrys, Chromium complexes of uric acid—synthesis, structure, and properties, Journal of Inorganic Biochemistry 48 (1992) 85-93. https://doi.org/10.1016/01620134(92)80018-Q

[16] Ruth Stephanie, Dae Yeon Lee, Chan Yeong Park and Tae Jung Park, Transition metal complex-incorporated polyaniline as a platform for an enzymatic uric acid electrochemical sensor, Analyst, 148 (2023) 1442-1450. https://doi.org/10.1039/D3AN00014A

[17] N. Reeshemah Allen, M. K. Shukla, V. Jaroslav Burda, J. Jerzy Leszczynski, Theoretical Study of Interaction of Urate with Li+, Na+, K+, Be2+, Mg2+, and Ca2+ Metal Cations, Phys. Chem. A, 110 (2006) 6139-6144. https://doi.org/10.1021/jp0603379

[18] Jill K. Wolken, Frantisek Turecek, Proton affinity of uracil. A computational study of protonation sites, J. Am. Soc Mass spectrometry, 11 (2000) 1065-1071.

https://doi.org/10.1016/S10440305(00)00176-8

[19] Caroline L. Benn, Pinky Dua, Rachel Gurrell, Peter Loudon, Andrew Pike, R. Ian Storer, Ciara Vangjeli, Physiology of Hyperuricemia and Urate-Lowering Treatments, Front Med (Lausanne), 160 (2018) 1-28 . https://doi.org/10.3389/fmed.2018.00160.

[20] Robert C. Smith a, Jeri Z. Gore a, Michael McKee, Howard Hargis, The first dissociation constant of uric acid, Microchemical Journal, 38 (1988) 118-124. https://doi.org/10.1016/0026265X(88)90010-0.

[21] V. Barone, M. Cossi, Quantum Calculation of Molecular Energies and Energy Gradients in Solution by a Conductor Solvent Model J. Phys. Chem. A, 1998, 102, 1995 -2001. https://doi.org/10.1021/jp9716997.

[22] M. Cossi, N. Rega, G. Scalmani, V. Barone, Energies, structures, and electronic properties of molecules in solution with the C-PCM solvation model J. Comp. Chem, 24 2003,669-681. https://doi.org/10.1002/jcc.10189

[23] A. E. Reed and P. R. Schleyer, Chemical bonding in hypervalent molecules. The dominance of ionic bonding and negative hyperconjugation over d-orbital participation J. Am. Chem. Soc , 112 (1990) 1434-1445. https://doi.org/10.1021/ja00160a022

[24] Olga Kovatchoukov, Neguissie Retta, Akalu Terfa, synthesis of complexes of uric acid with group I and II B Metals, Bull. Chem. Soc. Ethiop. 10 (1996) 39-42.

[25] Frisch, M.J.; Trucks, G.W.; Schlegel, H.B.; Scuseria, G.E.; Robb, M.A.; Cheeseman, J.R.; Scalmani, G.; Barone, V.; Petersson, G.A.; Nakatsuji, H.; et al. Gaussian 16, Revision A.03; Gaussian, Inc.: Wallingford, CT, USA, 2016.

[26] A.D. Becke, Density-functional thermochemistry. I. The effect of the exchange-only gradient correction. J. Chem. Phys. 96 (1992) 2155–2160. https://doi.org/10.1063/1.462066

[27] C.T.Lee,; W.T.Yang,; R.G. Parr, Development of the Colle-Salvetti Correlation-Energy Formula into a Functional of the Electron-Density. Phys. Rev. B 37 (1988) 785–789. https://doi.org/10.1103/PhysRevB.37.785

[28] G.Scalmani,; M. J. Frisch, Continuous Surface Charge Polarizable Continuum Models of Solvation. I. General Formalism. J. Chem. Phys. 132 (2010) 114-110. https://doi.org/10.1063/1.3359469

[29] K. Wolinski, K.J.F. Hilton, P. Pulay, Efficient implementation of the gauge-independent atomic orbital method for NMR chemical shift calculations, J. Am. Chem.

Soc. 112 (1990) 8251-8260. https://doi.org/10.1021/ja00179a005

[30] Minh Tho Nguyen, Asit K. Chandra Therèse Zeegers-Huyskens, Protonation and deprotonation energies of uracil Implications for the uracil–water complex, J. Chem. Soc., Faraday T rans, 94 , (1998) 1277-1280. https://doi.org/10.1039/A708804C

[31] Michal Trachta, Roman Bulánek, Ota Bludský , Miroslav Rubeš, Brønsted acidity in zeolites measured by deprotonation energy, scientific reports, 2022, 12:730. https://doi.org/10.1038/s41598-022-11354-x

[32] V. Jiménez, J. B. Alderete, Theoretical calculations on the tautomerism of uric acid in gas phase and aqueous solution. Journal of Molecular Structure: THEOCHEM. 755 (2005) 209–214. https://doi.org/10.1016/j.theochem.2005.08.001

[33] G. Schubert, R. Gunter, H. Jancke, W. Kraus, C. Patzelt, Uric acid monohydrate—A new urinary calculus phase. Urol. Res. 33 (2005) 231–238. https://doi.org/10.1007/s00240-005-0467-5

[34] R. Alina Izatulina, V. Vladislav Gurzhiy , G. Maria Krzhizhanovskaya, V. Nikita Chukanov, L. Taras Panikorovskii , Thermal Behavior and Phase Transition of Uric Acid and Its Dihydrate Form, the Common Biominerals Uricite and Tinnunculite. Minerals, 373 (2019) 1-13. https://doi.org/10.3390/min9060373

[35] R. N. Allen, M. K Shukla, J. Leszczynski, Int. J. Quantum Chem. 100 (2004) 801-809. https://doi.org/10.1002/qua.20246

[36] Delano P Chong Theoretical Study of Uric Acid and its Ions in Aqueous Solution, J Theor Comput Sci, 104 (2013) 1-7 https://doi.org/ 10.4172/2376-130X.1000104

[37] Ion Alexandru Bobulescu and W. Orson Moe, Renal Transport of Uric Acid: Evolving Concepts and Uncertainties, Adv Chronic Kidney Dis. 2012 358–371. https://doi.org/10.1053/j.ackd.2012.07.009.

[38] M. Aichi, M. Hafied, A. Dibi, Journal of Structural Chemistry, theoretical study of pentavalent halosiliconates: structure and charge. 62 (2021) 824-834 https://doi.org/10.1134/S0022476621060020

[39] M. Aichi, M.Hafied, basicity and nucleophilicity effect in charge transfer of ALH3-Base adducts: theoretical approach 17 (2023) 221–236. https://doi.org/10.23939/chcht17.02.221